

BCSJ Award Article

In Situ Scanning Tunneling Microscopy Observation of Metal–Cluster Redox Interconversion and CO Dissociation Reactions at a Solution/Au(111) Interface

Hiroyuki Noda,[1] Hiromitsu Uehara,[1] Masaaki Abe,*[2] Takayuki Michi,[1] Masatoshi Osawa,*[3] Kohei Uosaki,*[1,4] and Yoichi Sasaki*[1,3]

[1]Division of Chemistry, Graduate School of Science, Hokkaido University, Kita-ku, Sapporo 060-0810

[2]Department of Applied Chemistry, Graduate School of Engineering, Kyushu University, Nishi-ku, Fukuoka 819-0395

[3]Catalysis Research Center, Hokkaido University, Kita-ku, Sapporo 001-0021

[4]International Center for Materials Nanoarchitectonics Satellite (MANA), National Institute for Materials Science (NIMS), Kita-ku, Sapporo 060-0810

Received March 2, 2009; E-mail: mabe@mail.cstm.kyushu-u.ac.jp

We present here an in situ scanning tunneling microscopy (STM) study of potential-induced reactions of oxo-centered acetato-bridged triruthenium clusters on Au(111) under electrochemical conditions, in which (i) reversible interconversion between two different redox states of the cluster and (ii) spontaneous dissociation of CO from the cluster were probed and visualized. It is known that the triruthenium complex $[Ru_3(\mu_3\text{-}O)(\mu\text{-}CH_3COO)_6(CO)(4\text{-methylpyridine})\{(NC_5H_4)\text{-}CH_2NHC(O)(CH_2)_{10}S\}]$ (**1**), which is in the mixed-valent $\{(Ru^{II}\text{–}CO)Ru^{III}Ru^{III}\}$ state, on Au(111) is one-electron oxidized to cationic complex $\mathbf{1}^+$ which corresponds to a $\{(Ru^{III}\text{–}CO)Ru^{III}Ru^{III}\}$ oxidation state. The redox reaction is reversible on a cyclic voltammetry timescale. Complex $\mathbf{1}^+$ undergoes irreversible dissociation of CO in an aqueous phase on a longer timescale (ca. minutes) to form an aqua ligand-coordinated complex, $\mathbf{2}^+$, which is expressed as $\{(Ru^{III}\text{–}OH_2)Ru^{III}Ru^{III}\}$. The reversible redox reaction ($\mathbf{1} \rightleftarrows \mathbf{1}^+$) and the irreversible ligand substitution reaction ($\mathbf{1}^+ \rightarrow \mathbf{2}^+$) were independently examined with in situ STM in a monolayer level by visualizing molecular-sized spots showing a different extent of brightness in STM images. We show here that the molecular-sized spots corresponding to **1**, $\mathbf{1}^+$, and $\mathbf{2}^+$ are resolved by their brightness, which strongly depends on both the oxidation states and the ligand nature of the clusters. By employing multiple fast scans at an applied potential of +0.80 V vs. Ag/AgCl, we obtained STM images that follow the irreversible $\mathbf{1}^+ \rightarrow \mathbf{2}^+$ reaction on the surface, from which a rate constant of the CO release was calculated to be 1.9 ($\pm$0.2) $\times$ 10^{-2} s^{-1} (25 °C; in contact with 0.1 mol dm^{-3} aqueous $HClO_4$ solution). The difference in brightness of the molecular spots is rationalized in terms of orbital-mediated tunneling by considering the difference in electronic states of the dπ–pπ system in the μ_3-O triruthenium cluster.

Direct probe and analysis of atomic and molecular processes that occur at solid–solution interfaces have become increasingly essential for nanometer-scale science and technology. One crucial experimental challenge is to develop practical methods that allow direct observation of chemical reactions at a molecular or monolayer level. Scanning tunneling microscopy (STM) is a powerful technique for structural characterization of atoms, molecules, and supramolecular assemblies on surfaces and the enormous utility has been particularly manifested in probing atomic-scale processes in ultrahigh-vacuum.[1–5] While the in situ technique of STM has recently seen rapid progress for structural identification of molecules on well-defined electrode surfaces,[6–14] direct probe of chemical reactions which are triggered by applied potentials still remains a significant challenge.

In this paper, we describe a successful probe and analysis of potential-induced chemical reactions of self-assembled monolayers (SAMs) of an oxo-centered acetato-bridged trinuclear ruthenium cluster[15,16] $[\{Ru_3(\mu_3\text{-}O)(\mu\text{-}CH_3COO)_6(mpy)(CO)\}_2(\mu\text{-}C_{10}py)]$ (mpy = 4-methylpyridine, $C_{10}py = \{(NC_5H_4)CH_2NHC(O)(CH_2)_{10}S\}_2$) (Figure 1a)[17] at a solution/Au(111) interface with the in situ STM technique. Interfacial reactions examined here are illustrated in Figure 1b. The reactions involve two steps: (i) reversible interconversion between two different oxidation states **1** and $\mathbf{1}^+$ and (ii) irreversible spontaneous dissociation of a coordinated CO from $\mathbf{1}^+$ to yield $\mathbf{2}^+$. Both reactions are triggered by stringent control of applied potentials of the Au(111) working electrode. Here, **1** represents a carbonyl complex $[Ru_3(\mu_3\text{-}O)(\mu\text{-}CH_3COO)_6(mpy)(CO)\{(NC_5H_4)CH_2NHC(O)(CH_2)_{10}S\}]$ and $\mathbf{1}^+$ is the one-electron-oxidized form of **1**, while $\mathbf{2}^+$ represents a cat-

Published on the web October 8, 2009; doi:10.1246/bcsj.82.1227

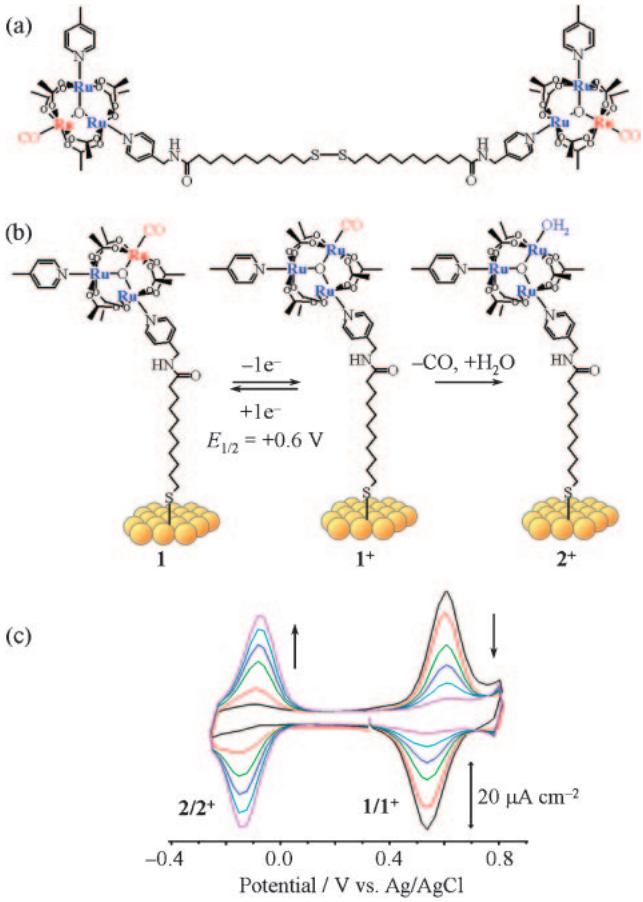

Figure 1. (a) Molecular structure of a triruthenium complex used in this study. (b) Schematic illustration of electrode potential-induced reactions examined in this study. (c) Ligand substitution reaction followed by cyclic voltammetry. Electrolyte solution: a 0.1 mol dm^{-3} aqueous $HClO_4$ solution. Scan rate: 0.5 V s^{-1}. Each cyclic voltammogram is recorded after electrolysis (+0.8 V vs. Ag/AgCl) of 0 (black), 20 (red), 50 (green), 90 (blue), 360 (light blue), and 3600 s (purple).

ionic aqua complex $[Ru_3(\mu_3\text{-}O)(\mu\text{-}CH_3COO)_6(mpy)(H_2O)\{(NC_5H_4)CH_2NHC(O)(CH_2)_{10}S\}]^+$ and **2** is its one-electron-reduced form. As our earlier studies have shown,[17,18] the CO dissociation from the cluster moiety is kinetically followed by cyclic voltammetry because redox potentials of the two redox couples, $\{\mathbf{1}/\mathbf{1}^+\}$ and $\{\mathbf{2}/\mathbf{2}^+\}$, are well separated and independently quantified, as shown in Figure 1c. It appears in this work that the surface-assembled cluster **1** and the electrochemically generated clusters $\mathbf{1}^+$ and $\mathbf{2}^+$ are distinctly visualized as molecular-sized spots with different brightness in STM images. The difference in brightness is discussed in terms of orbital-mediated tunneling through the triruthenium cluster groups involving different oxidation levels and terminal ligands. The noticeable visibility of the individual redox cluster components enabled us to observe reversible redox ($\mathbf{1} \rightleftarrows \mathbf{1}^+$) and irreversible ligand substitution reactions ($\mathbf{1}^+ \rightarrow \mathbf{2}^+$) at a monolayer level. In particular, the work is the first example of direct imaging and kinetic analysis of ligand-substitution reactions on surface-confined transition-metal complexes by using in situ STM.

Experimental

Materials. Complex $[\{Ru_3(\mu_3\text{-}O)(\mu\text{-}CH_3COO)_6(mpy)(CO)\}_2(\mu\text{-}C_{10}py)]$ (Figure 1a) was prepared as reported previously.[18] Water used for the electrolyte preparation was purified by using a Milli-Q water purification system (Simpli Lab, Millipore). All other chemicals were purchased and used without further purification.

Preparation of Au(111) Substrates and SAMs. A single-crystal Au bead was prepared at the end of a Au wire (99.99%; 0.8 mm in diameter). The (111) facet on the single-crystal Au bead in an octahedral configuration was used for the STM measurements. The Au(111) surface was cleaned before SAMs fabrication by flame annealing followed by quenching in H_2-saturated water.

The SAMs of **1** was prepared by immersing the clean Au(111) electrode into a freshly prepared ethanol solution of $[\{Ru_3(\mu_3\text{-}O)(\mu\text{-}CH_3COO)_6(mpy)(CO)\}_2(\mu\text{-}C_{10}py)]$ (10 μmol dm^{-3}) for 24 h. The SAMs-modified Au bead was thoroughly rinsed with ethanol and ultrapure water. The SAMs-coated Au(111) surface was covered with a drop of water to protect against contamination and it was transferred to a home-made electrochemical cell for the STM measurements.

In Situ STM Measurements. The constant-current STM images were obtained with a Nanoscope E (Digital Instruments, Santa Barbara, CA) at room temperature. The electrochemical cell with four-electrode configuration was used for in situ STM experiments, in which the electrode potentials of the tunneling tip (an electrochemically-etched tungsten wire with a coat of transparent nail polish) and the Au(111) substrate were independently controlled. A platinum coil and a platinum wire were used as a counter electrode and a reference electrode, respectively. All the electrode potentials in this paper are reported with respect to Ag/AgCl. For a bare Au(111) electrode which we prepared, a well-defined terrace-step structure with a hexagonal close-packed Au atom alignment was confirmed by in situ STM in an aqueous solution containing 0.1 mol dm^{-3} $HClO_4$.

Electrochemistry of the SAMs. A series of CVs shown in Figure 1c was obtained using an Au(111) electrode (the surface area, 0.08 cm^2) covered with densely-packed SAMs of **1** which was prepared as described previously.[17,18] A platinum coil and Ag/AgCl (saturated NaCl) were used as a counter electrode and a reference electrode, respectively. An aqueous solution of 0.1 mol dm^{-3} $HClO_4$ was used as an electrolyte. To promote the CO dissociation from surface-confined **1**, the applied potential was held at +0.8 V vs. Ag/AgCl to form $\mathbf{1}^+$, and CVs were recorded at a certain time interval in the potential region between +0.8 and −0.3 V at a scan rate of 0.5 V s^{-1}. The potential-holding and the CV measurement were repeated until the CV no longer changed, where the principal surface-confined species are $\mathbf{2}^+$. The amount of redox species on the electrode surface was calculated from charge under the redox wave at +0.60 V for **1** ($\mathbf{1}^+$) and that at −0.15 V for **2** ($\mathbf{2}^+$). The CV recording was performed at room temperature with a Hokuto Denko HA-301 electrochemical system.

Results and Discussion

Surface Structure of 1 Adsorbed on a Au(111) Electrode. The SAMs of **1** on Au(111) show a reversible redox wave at the half-wave potential ($E_{1/2}$) of +0.60 V vs. Ag/AgCl in contact with an aqueous solution of 0.1 mol dm^{-3} $HClO_4$ (see the initial CV (a black curve) in Figure 1c). This redox couple is ascribed to a one-electron exchange between the neutral $\{(Ru^{II}\text{–}CO)$-

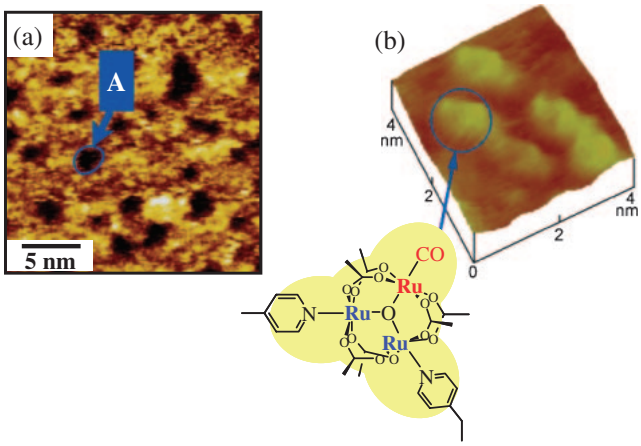

Figure 2. In situ STM images of monolayers of **1** on Au(111) in contact with 0.1 mol dm^{-3} at room temperature. $V_{Au} = +0.20$ V, $V_{tip} = -0.05$ V, and $I_{tc} = 0.3$ nA. (a) A 20×20 nm^2 region. Symbol "A" shows a vacancy island. (b) A 4×4 nm^2 region. For the sake of clarity, one of the molecular spots is highlighted with an illustration of the triruthenium cluster.

$Ru^{III}Ru^{III}\}^0$ state (**1**) and the cationic $\{(Ru^{III}–CO)Ru^{III}Ru^{III}\}^+$ state (**1**$^+$).[17–19] The redox process is reversible on a cyclic voltammetry timescale. Complex **1**$^+$ on the surface is however not stable if the applied potential is set at +0.8 V for longer time (ca. minutes), dissociating CO from the cluster moiety to yield **2**$^+$ in the $\{(Ru^{III}–OH_2)Ru^{III}Ru^{III}\}^+$ state.[17,18]

First, we examined molecular images of **1** on Au(111) in 0.1 mol dm^{-3} $HClO_4$ solution. Figure 2a shows a typical STM image, in which the potential of the Au(111) substrate (V_{Au}) is held at +0.20 V so that the complex exists as **1** in the $\{(Ru^{II}–CO)Ru^{III}Ru^{III}\}^0$ form. As shown, the entire tip-scanned surface is covered densely with grained spots. These spots are ascribed to the triruthenium cluster molecules adsorbed on the Au(111) surface (see later). Shown as "A" in Figure 2a are so-called "vacancy islands," which are formed by thiol-mediated etching of Au.[6] The individual bright spots are more clearly visible in a high-resolution STM image (4×4 nm^2) as shown in Figure 2b, which is a typical image found on any surface area of the SAMs sample of **1**. The diameter of the spots is estimated to be ca. 1.0 nm which is in reasonable agreement with that confirmed by X-ray crystallography of a triruthenium cluster derivative reported in literature.[20] It appears that the clusters are randomly distributed on the Au surface and no long-range ordered morphology is found. The ruthenium cluster moiety $\{Ru_3(\mu_3\text{-}O)(\mu\text{-}CH_3CO_2)_6L_3\}$ (L is a terminal ligand) in **1** is non-planar and seems unlikely to form ordered morphology due to molecule–molecule and/or molecule–substrate interactions.

Observation of Reversible Redox Interconversion by In Situ STM Measurements. The redox interconversion **1** $\rightleftarrows$ **1**$^+$ is reversible as long as the potential-stepping operation is conducted within 10 s, during which time the conversion from **1**$^+$ to **2**$^+$ is negligible. Figures 3a and 3b are representative images obtained over a larger scanning area (100×100 nm^2). These two images were successively obtained by scanning the tip from the top to the bottom region while $V_{Au} =$

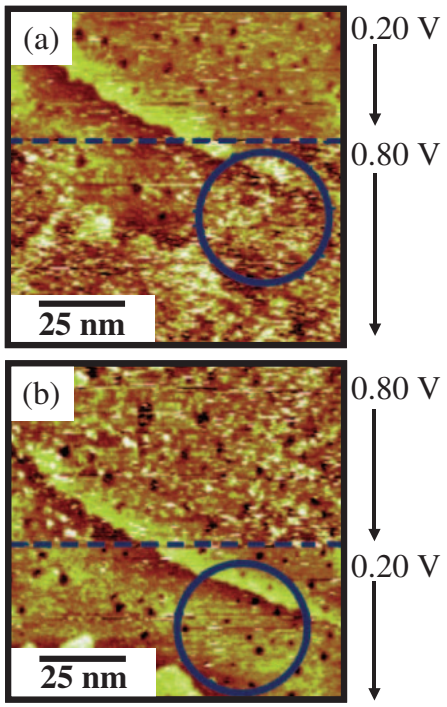

Figure 3. In situ STM images monitoring reversible redox interconversion recorded at different V_{Au}. (a) An STM image recorded initially at $V_{Au} = +0.20$ V to yield **1** followed by stepping the applied potential at $V_{Au} = +0.80$ V to yield **1**$^+$ as a major surface species. (b) An STM image recorded at $V_{Au} = +0.80$ V and stepped back to $V_{Au} = +0.20$ V. The V_{Au} is shown in the right side of each figure. The V_{tip} was −0.05 V.

+0.20, +0.80, and +0.20 V was applied to form **1**, **1**$^+$, and again **1**, respectively. By stepping the potential from $V_{Au} = +0.20$ to +0.80 V (a broken line in Figure 3a), brighter spots are visible on the surface, the change which should be ascribed to the one-electron oxidation of **1** to form **1**$^+$. This observation indicates that **1**$^+$ shines more brightly than **1** does. Stepping back the potential to +0.20 V (a broken line in Figure 3b) regenerated the initial image. It should be noted that, in order to minimize effects of the irreversible formation of **2**$^+$, a fast scan of the STM tip (typically 5 nm s^{-1} in the y axis direction) was employed to observe the redox interconversion between **1** and **1**$^+$, although the fast scanning gave less clear images (Figure 3). A stripe feature is also observed along the x axis direction. However, the present observations are still striking in that interfacial redox reactions and ligand substitution reactions of transition-metal complexes become visible by observing a contrast change in the STM image that distinctly reflects redox states and ligand nature (see later) of the molecular units on the surface.

Observation of Irreversible CO Dissociation and Kinetic Analysis by In Situ STM Measurements. We next sought to observe the irreversible, spontaneous dissociation of CO from **1**$^+$ which occurs at $V_{Au} = +0.80$ V over a longer timescale (ca. minutes). As shown in Figure 4, bright spots due to **1**$^+$, which are visible as pale pink, decreased as the time progressed. It should be noted that the STM images presented in Figure 4 are rather not clear in the context of resolution. This is due in part

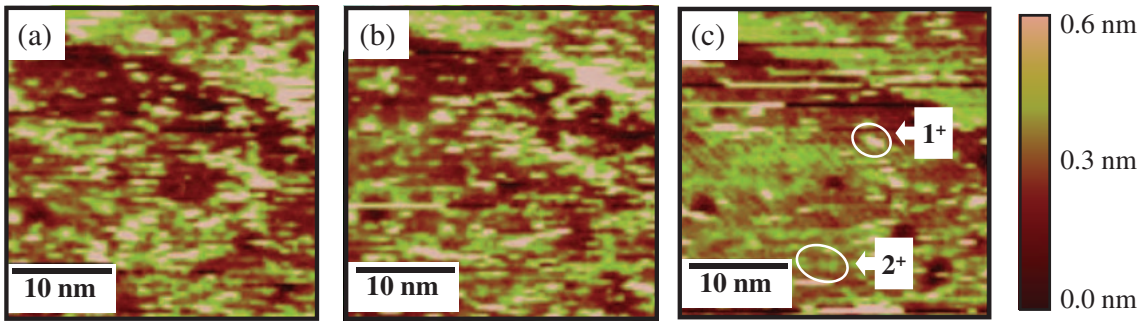

Figure 4. In situ STM images ($V_{tip} = -0.05$ V, $I_{tc} = 0.3$ nA) monitoring irreversible, spontaneous CO dissociation from $\mathbf{1}^+$ at $V_{Au} = +0.80$ V. STM images are obtained after the potential holding of 80 (a), 100 (b), and 160 s (c). 7 s was required for recording each image. The region is identical to the encircled area in Figure 3.

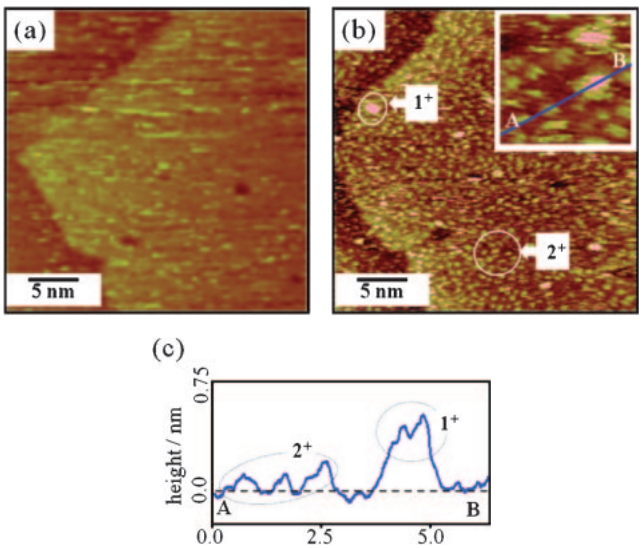

Figure 5. High-resolution STM images recorded before and after electrolysis (7 min) at a slower tip scan rate (0.1 nm s^{-1}). (a) Before electrolysis ($V_{Au} = +0.30$ V, $V_{tip} = -0.30$ V): **1** is a major species on the surface. (b) After electrolysis ($V_{Au} = +0.80$ V, $V_{tip} = -0.30$ V): $\mathbf{2}^+$ is a major species and $\mathbf{1}^+$ is a minor species on surface. Inset: A 5×5 nm^2 region. (c) Cross-sectional analysis along A–B line indicated in the inset of Figure 5b.

to a fast tip-scan that we employed to record the surface reaction occurring within minutes and also due to technical difficulty in obtaining high-resolution (molecular resolution) images of sterically non-planar molecules under electrochemical conditions. After multiple efforts however, we were able to obtain higher-resolution STM images where **1**, $\mathbf{1}^+$, and $\mathbf{2}^+$ became visible in different brightness. Figures 5a and 5b are STM images recorded before electrolysis and after electrolysis of 7 min, respectively, at the same surface area with a slower tip scan rate. Spots ascribed to **1** are visible over the entire surface in Figure 5a while in Figure 5b major surface species ascribed to $\mathbf{2}^+$ are observed together with minor but brighter spots ascribed to $\mathbf{1}^+$ (which most probably are still unreacted at the time of observation). A cross-sectional height profile shown in Figure 5c obtained from Figure 5b, inset, indicates the two components.

The time-dependent STM contrast change presented in Figure 4 motivated us to analyze the CO dissociation reaction

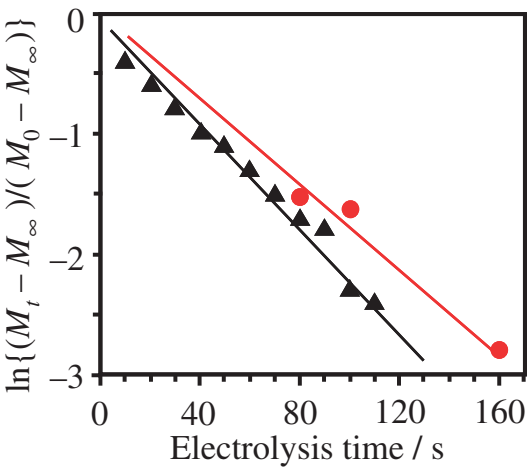

Figure 6. The first-order plots of the CO dissociation reaction. A red line represents the plot obtained from Figures 4a–4c, while a black line is generated from CVs shown in Figure 1c. For STM data, a plot of $\ln\{(M_t - M_\infty)/(M_0 - M_\infty)\}$ against electrolysis time (t) is shown, where M_0, M_t, and M_∞ are the number of spots assigned to $\mathbf{1}^+$ at $t = 0$, t, and ∞, respectively.

of $\mathbf{1}^+$ kinetically. The first-order kinetic treatment for the spots due to $\mathbf{1}^+$, shown as red in Figure 6, gave a rate constant of 1.9 ($\pm$0.2) $\times$ 10^{-2} s^{-1} (25 °C; see the Supporting Information for more details). By considering rather large margins of error of the present STM images, the kinetic plot obtained is similar to those obtained from cyclic voltammetry (presented as black in Figure 6) using Figure 1c.[17,18] This similarity shows that surface kinetic reactions are followed by the in situ STM measurement as far as they take place at a timescale of minutes.

An STM Image Contrast of 1, $\mathbf{1}^+$, and $\mathbf{2}^+$ on Au(111). The observed contrast change in the STM images reflects the change in the electronic configuration of **1**, $\mathbf{1}^+$, and $\mathbf{2}^+$. Replacement of CO with H_2O leads to a significant modulation of the energy of Ru d-orbitals, which eventually causes tunneling current to vary. It is reported that the contrast of STM images of redox molecules is highly dependent on the tunneling probability associated with the electronic configuration of the molecules, which is successfully explained in terms of orbital-mediated tunneling.[21,22] In the case of triruthenium clusters, molecular orbitals (MOs) are constructed by dπ orbitals on each Ru atom and a pπ orbital of the central

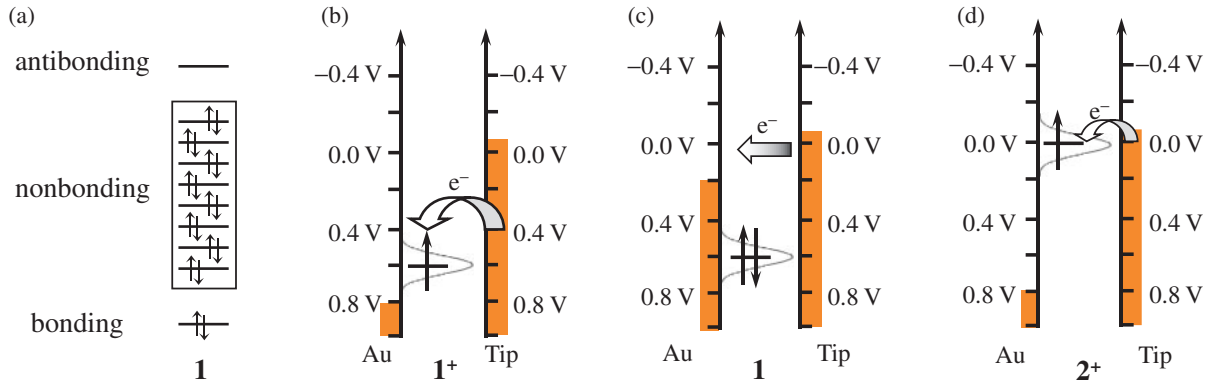

Figure 7. (a) A qualitative MO diagram of **1**. (b) to (d) Schematic of relative potential energy of the substrate potential (V_{Au}), tip potential (V_{tip}), and HOMO (or SOMO) in $\mathbf{1}^+$ (b), **1** (c), and $\mathbf{2}^+$ (d) with the corresponding electron configurations.

μ_3-oxo ion.[15,23] As shown in Figure 7a, simplified MOs consist of one bonding orbital, eight nonbonding orbitals, and one antibonding orbital. For **1**, the bonding and non-bonding orbitals are fully occupied, whereas one-electron oxidation of **1** forms the half occupied non-bonding orbital. We consider that $\mathbf{1}^+$ shines brightly because the half-filled orbital effectively serves as the tunneling pathway (Figure 7b). Such an effect, however, is no longer expected for **1** due to the full occupation of the HOMO (Figure 7c). For $\mathbf{2}^+$ (Figure 7d), the semi-occupied molecular orbital (SOMO) again allows tunneling current to flow resonantly but with a different extent due to the orbital energy difference between $\mathbf{1}^+$ and $\mathbf{2}^+$. It is noted that in the STM image of $\mathbf{2}^+$ the brightness of the individual spots depends on the tip potential; the brightness was highly enhanced when the tip potential was shifted from −0.05 to −0.30 V.

Conclusion

In conclusion, electrode potential-induced reactions of surface-confined metal cluster compounds have been successfully observed and kinetically analyzed by use of an in situ STM technique. In spite of low-resolution images obtained at a faster tip scanning under conditions studied, the time-dependent images allowed us to study dynamics and kinetics of redox-induced chemical reactions. This illustrates a remarkable utility of in situ STM as a tool for kinetic analysis of coordination reactions at a monolayer level, particularly those induced by applied potentials under electrochemical conditions.

This work was partly supported by Grant-in-Aid for Scientific Research on Priority Area "Reaction Control of Dynamic Complexes," "Chemistry of Coordination Space," and "Chemistry of Concerto Catalysis" (Nos. 16033201, 17036002, and 19028002, respectively), Grant-in-Aid for Scientific Research B (No. 20350029), and the Global COE Programs "Catalysis as the Basis for Innovation in Material Science" and "Science for Future Molecular Systems" from the Ministry of Education, Culture, Sports, Science and Technology of Japan. H.N. acknowledges fellowship from the Japan Society for the Promotion of Science (JSPS).

Supporting Information

Time-dependent change in the number of molecular spots of $\mathbf{1}^+$ on STM images used for the kinetic analysis. This material is available free of charge on the web at http://www.csj.jp/journals/bcsj/.

References

1 J. Wintterlin, S. Völkening, T. V. W. Janssens, T. Zambelli, G. Ertl, *Science* **1997**, *278*, 1931.
2 J. K. Gimzewski, C. Joachim, *Science* **1999**, *283*, 1683.
3 X.-C. Guo, R. J. Madix, *J. Phys. Chem. B* **2003**, *107*, 3105.
4 S. W. Wu, N. Ogawa, G. V. Nazin, W. Ho, *J. Phys. Chem. C* **2008**, *112*, 5241.
5 S. Katano, Y. Kim, H. Matsubara, T. Kitagawa, M. Kawai, *J. Am. Chem. Soc.* **2007**, *129*, 2511.
6 R. Yamada, K. Uosaki, *Langmuir* **1997**, *13*, 5218.
7 R. Yamada, K. Uosaki, *Langmuir* **1998**, *14*, 855.
8 K. Uosaki, R. Yamada, *J. Am. Chem. Soc.* **1999**, *121*, 4090.
9 B. Ohtani, A. Shintani, K. Uosaki, *J. Am. Chem. Soc.* **1999**, *121*, 6515.
10 H. Naohara, S. Ye, K. Uosaki, *J. Phys. Chem. B* **1998**, *102*, 4366.
11 S. Yoshimoto, N. Hirakawa, K. Nishiyama, I. Taniguchi, *Langmuir* **2000**, *16*, 4399.
12 K. Itaya, *Prog. Surf. Sci.* **1998**, *58*, 121.
13 S. Ye, T. Kondo, N. Hoshi, J. Inukai, S. Yoshimoto, M. Osawa, K. Itaya, *Electrochemistry* **2009**, *77*, 2.
14 Y. Yokota, K. Fukui, T. Enoki, M. Hara, *J. Phys. Chem. C* **2007**, *111*, 7561.
15 Y. Sasaki, M. Abe, *Chem. Rec.* **2004**, *4*, 279.
16 M. Abe, *Bull. Jpn. Soc. Coord. Chem* **2004**, *44*, 11.
17 A. Sato, M. Abe, T. Inomata, T. Kondo, S. Ye, K. Uosaki, Y. Sasaki, *Phys. Chem. Chem. Phys.* **2001**, *3*, 3420.
18 T. Michi, M. Abe, J. Matsuno, K. Uosaki, Y. Sasaki, *Bull. Chem. Soc. Jpn.* **2007**, *80*, 1368.
19 S. Ye, H. Akutagawa, K. Uosaki, Y. Sasaki, *Inorg. Chem.* **1995**, *34*, 4527.
20 M. Abe, Y. Sasaki, Y. Yamada, K. Tsukahara, S. Yano, T. Yamaguchi, M. Tominaga, I. Taniguchi, T. Ito, *Inorg. Chem.* **1996**, *35*, 6724.
21 L. Scudiero, D. E. Barlow, U. Mazur, K. W. Hipps, *J. Am. Chem. Soc.* **2001**, *123*, 4073.
22 S. Yoshimoto, E. Tsutsumi, K. Suto, Y. Honda, K. Itaya, *Chem. Phys.* **2005**, *319*, 147.
23 C. H. Londergan, C. P. Kubiak, *J. Phys. Chem. A* **2003**, *107*, 9301.